Results in Chemistry 5 (2023) 100851

Contents lists available at ScienceDirect

Results in Chemistry

journal homepage: www.sciencedirect.com/journal/results-in-chemistry

Removal of Cu (II) *via* chitosan-conjugated iodate porous adsorbent: Kinetics, thermodynamics, and exploration of real wastewater sample

Aloysius Akaangee Pam [a,*], Olugbenga Oluseun Elemile [b], Dallatu Ephraim Musa [a], Maureen Chijoke Okere [b], Amos Olusegun [c], Yakubu Ahmed Ameh [d]

[a] Department of Chemistry, Faculty of Science, Federal University Lokoja, Lokoja, Nigeria
[b] Civil Engineering Department, College of Engineering, SDG 6 (Clean Water and Sanitation Research Group) Landmark University, Omu-Aran, Kwara State, Nigeria
[c] Department of Chemistry, School of Physical Sciences, Federal University of Technology Owerri, Imo State, Nigeria
[d] Department of Environmental Management, School of Environmental Sciences, Federal University of Technology, Owerri, Nigeria

ARTICLE INFO

Keywords:
Chitosan
Iodate doped chitosan
Adsorption
Regeneration
Copper

ABSTRACT

Remediation of copper (II) pollutant in aquatic ecosystems is a long-standing concern in the field of water management and the subject of intensive research. In this study, chitosan conjugated iodate porous material (CS-CI) was successfully prepared by media (ammonia, acetic acid, and absolute ethanol) and was used in the treatment of Cu (II) in wastewater samples. Different methods were applied to characterize the CS-CI, including FTIR, SEM, XRD, and TGA. The result showed significant improvement in surface properties and stability when the chitosan was conjugated with the iodate. The adsorption of Cu (II) followed the pseudo-first-order kinetic model and Langmuir isotherm model with a maximum adsorption capacity of 95.2 mg/g. In a complex system (real wastewater), the CS-CI took advantage of the adsorptive properties of both chitosan (CS) and the iodate to significantly improved the remediation of Cu (II) in aqueous media. Therefore, the synthesized chitosan conjugated iodate porous material is promising as an alternative low-cost adsorbent for the treatment of copper (II) in wastewater.

Introduction

Global contamination of water bodies with pollutants has challenged researchers worldwide to find newer, less expensive treatments. There are many ways in which water bodies are polluted, but effluent pollution from industrial installations is still the most important [1]. The pollution of water by effluents containing heavy metal ions from various manufacturing industries pose a serious ecological problem. Copper (Cu) is one of the metals frequently detected in surface water and wastewater, and has a high ecological and toxicity risk, with an allowable limit of 2.0 mg/L according to the World Health Organization (WHO) [2]. Human activities (copper plating, mining, smelting, metal processing, and the use of Cu in agriculture as a fungicide) discharge copper-laden wastewater into ecosystems, reducing soil and water quality while increasing human exposure risk [3]. Exposure to elevated concentration of Cu (II) has grave toxicological effects to health of human including Wilson's and liver disease [3], or even death. Hence, it becomes important that water-containing copper be treated before sending to receiving water bodies. A number of techniques have been proposed for Cu (II) removal from wastewater including ion exchange, chemical precipitation, electrolysis, and membrane filtration. However, high energy cost, low efficiency at high organic load and low effluent concentration, slow response, and sensitivity are some of the disadvantages of such methods [4]. Adsorption using adsorbent is considered most efficient, economic, and widely used technique [5] Adsorbents such as ion exchange resins [6], carbon-based nanomaterials [7], mesoporous silica [8], and zeolites [9] have demonstrated their ability to act as adsorbents for the treatment of Cu (II) in aqueous environment. However, the extensive use of many of these adsorbents is limited by low metal ion selectivity [10], low adsorption capacity [11], high cost, and structurally difficult to achieve chemical modification. Consequently, research into novel adsorbent materials with low fabrication cost, superior physical and structural properties, high adsorption capacity, chemically diverse [12], biodegradable, and easily modified adsorbents has been intensified. Chitosan (β-(1–4)-D-glucosamine) derivatives have increasingly demonstrated to solve some of these problems due to the existence of amino ($-NH_2$) and hydroxyl ($-OH$) functional groups in chitosan. Chitosan (CS), a biopolymer, is a polysacrides that possess two

* Corresponding author at: Chemistry Department, Faculty of Science, Federal University Lokoja, P.M.B. 1154, Lokoja, Nigeria.
E-mail address: aloysius.pam@fulokoja.edu.ng (A. Akaangee Pam).

https://doi.org/10.1016/j.rechem.2023.100851
Received 28 December 2022; Accepted 9 February 2023
Available online 14 February 2023

types of monomers, an acetamindo group (2–acetamido–2–deoxy-D–glucopyranose residues) and amino group (2–amino–2–deoxy-D–glucopyranose residues) [4,13]. However, using CS in powder or flake form is challenging due to its resistance to mass transfer, high crystallinity, low porosity, low chemical/thermal stability, low reusability, and low surface area [14]. In addition to combining chitosan with other adsorbents to overcome these disadvantages, chemical and structural modifications involving grafting and cross-linking have also been proposed [14]. Apart from the CS having amino ($-NH_2$) and hydroxyl ($-OH$) functional groups, the micropolymer is capable of forming positive charges, making it useful for chemical conjugates with many anionic substrates [15]. When combined with anionic substrates, CS exhibits many properties superior to bulk CS materials, including improved selectivity and enhanced metal-binding capacity as well as improved mechanical and thermal stability. Hence, these properties and their optimization are key to the formation of highly efficient adsorbents [4]. It is on this basis that the chitosan conjugated iodate porous material (CS-CI) was developed. At low pH, the NH_2 groups in CS are protonated (NH_3^+), and the IO_3^- anion will now conjugate with the positive charges on CS to form chitosan-conjugated iodate ($NH_3^+IO_3^-$) porous adsorbent. The electrostatic attraction between opposite charges and hydrogen-bonding interactions maximizes the mechanical and chemical stability of the CS-CI, which facilitates reusability and increased diversity of chemical functionalities without conceding the pollutant removal efficiency. The main factors to be considered in the formation and stability of the conjugate are CS concentration, pH of the reaction medium, nature of possible interactions between different groups in the CS-iodate complex. The combination of chitosan and iodate as an adsorbent (CS-CI) in the treatment Cu (II) in simulated and real wastewater has not been previously considered. Therefore, the synthesized CS-CI was characterized and the adsorption process was investigated; moreover, the effect of adsorbent dosage and pH value, kinetics and isotherm model were further investigated. Finally, single–solute and multi-solute test experiments were investigated.

Materials and methods

Synthesis of chitosan-conjugated iodate porous material(CS-CI)

The CS-CI was synthesized according to the same method reported previously [16] with little modification. To be precise, we added 2 g of chitosan flakes (75 % to 80 % deacetylation from chitin, with molecular weight 250,000 g/mol obtained from Sigma-Aldrich) to acetic acid (2 %, 100 mL) and then magnetically stirred the mixture (at 50 °C, 30 min) to obtain Homogeneous gel. Chitosan gel was then added to potassium iodate (KIO_3) (1:1 w/w) that was previously pretreated with ethanol (2:1) and stirred (500 rpm, 5 h). The resulting mixture was added drop by drop to 50 % aqueous ammonia, and the mixture was filtered and washed. The resulting adsorbent CS-CI was then dried in an oven at 60 °C for 24 h. The CS-CI was reduced in particle size using a pestle and mortar, passed through a 200-mesh sieve, and then put into a sample vial for further characterization and adsorption experiments.

Adsorbent characterization

The porosity information of the CS-CI were obtained through N_2 adsorption and desorption isotherm using BET (Brunauer-Emmet-Teller) and BJH(Barrett-Joyner-Halenda) methods (Micromeritics 3 Flex, USA) after previously degassing at 300 °C for 11 h. CS-CI micromorphology was investigated by scanning electron microscopy (SEM, FEI Nova 230). X-ray diffraction (XRD) spectrum of CS-CI was performed on Bruker/D5000 (Germany) powder diffractometer (at 26 mA with Cu $K\ \alpha$ radiation) with dataset collection ranging from 20 to 80° and 0.02/2θ step width. The thermal stability of CS-CI was investigated using a thermogravimetric analyzer (STA 600 Perkin Elmer) in the temperature range 0–900 °C at a heating rate of 10 °C min^{-1} under N_2 flow (100 mL/min). FTIR (Fourier Transform Infrared Spectroscopy) of CS-CI before and after Cu (II) treatment was recorded on Perkin Elmer attenuated reflection (ATR) spectrometer (PerkinElmer, USA) in the range of 400 to 4000 cm^{-1} with a resolution of 4 cm^{-1}. The point of zero charge (pH_{PZC}) was assessed by the pH drift method as described in our previous work [17]. The pHpzc value for this CS-CI is defined as the point where the ΔpH line intersects the x axis (initial pH), i.e. (pHf - pHi) = 0.0.

Experiment for Cu (II) adsorption

The stock solution of Cu (II) was obtained by dissolving stoichiometric amount of $CuCl_2{\cdot}2H_2O$ in 1000 mL deionized water. All other reagents used in this work were of analytical grade, including $CuCl_2{\cdot}2H_2O$, NaOH, HCl and were purchased from Sigma-Aldrich (St. Louis, MI, USA). Sequestration of Cu (II) in solution was performed by CS-CI in a 250 mL Erlenmeyer flask by varying the sorbent dosage and pH. Erlenmeyer flask containing 200 mL solution of Cu (II) was agitated at 150 rpm for 100 min in a water bath orbital shaker at constant temperature. To understand the mechanisms involved in the adsorption process, a suspension consisting 0.1g of CS-CI in 200 mL of a 125 mg/L Cu solution was agitated for 10–100 min. The pH of the initial solution of Cu (II) was adjusted to the range of 2–6 with HCl and NaOH. Construction of isotherms to assess the equilibrium absorption capacity of CS-CI for Cu (II) was achieved using 10 to 125 mg/L Cu (II) initial concentrations at 25 °C. All experimental sets were performed in duplicate, and the results obtained were analyzed as mean values. The absorption capacity and percent removal (%) at equilibrium are expressed by equations (1) and (2) [18,19].

$$q_e(mg/g) = \frac{(C_o - C_e)}{M} \times V \tag{1}$$

$$\text{Efficiency}\,(\%) = \frac{(C_o - C_e)}{C_o} \times 100 \tag{2}$$

where Co and Ce are the initial and equilibrium concentrations in mg/L, and V is Cu (II) solution used (L), *M* is the mass of CS-CI used in g.

Results and discussion

Adsorbent characterization

The surface morphology of CS and CS-CI are shown in Fig. 1 (a) and Fig. 1(b). After adding KIO_3, the smooth and polished structure of the CS is completely changed. The CS-CI showed a heterogeneous and porous surface with different pore sizes, which maximizes the specific surface area and reaction rate of the material. These porous structures facilitate swelling, allow diffusion of bulk Cu (II) ions and support interactions between iodate and Cu (II) ions in the wastewater sample, which is useful to improving the adsorption performance of the CS-CI. Hence, the prepared CS-CI is considered a promising candidate for water treatment applications. The N_2 isotherm CS-CI (Fig. 1(c)) was classified as type IV with a hysteresis loop observed at high relative pressure, indicating the existence of mesopores [20]. Besides, the BET specific surface area, PSD (Fig. 1(d)) and pore volume were 1.4991 m^2/g, 0.17324 cm^3/g and 2.171 nm, respectively.

Fig. 1(e) shows the pattern of powder XRD of the as-prepared CS-CI. The samples shows diffraction peaks corresponding 2θ values of 20.10°, 28.30°, 35.0°, 40.70°, 45.90° and 49.10°, respectively. Comparison of JCPDS standard card no. (01–072-1955) shows that the diffraction peaks are related to potassium iodate. Furthermore, the crystallinity of CS-CI was demonstrated by applying the Debye-Scherer equation (Eq. 3) [21].

$$\textit{Mean crystallite size}(D) = 0.89\lambda/\beta cos\theta \tag{3}$$

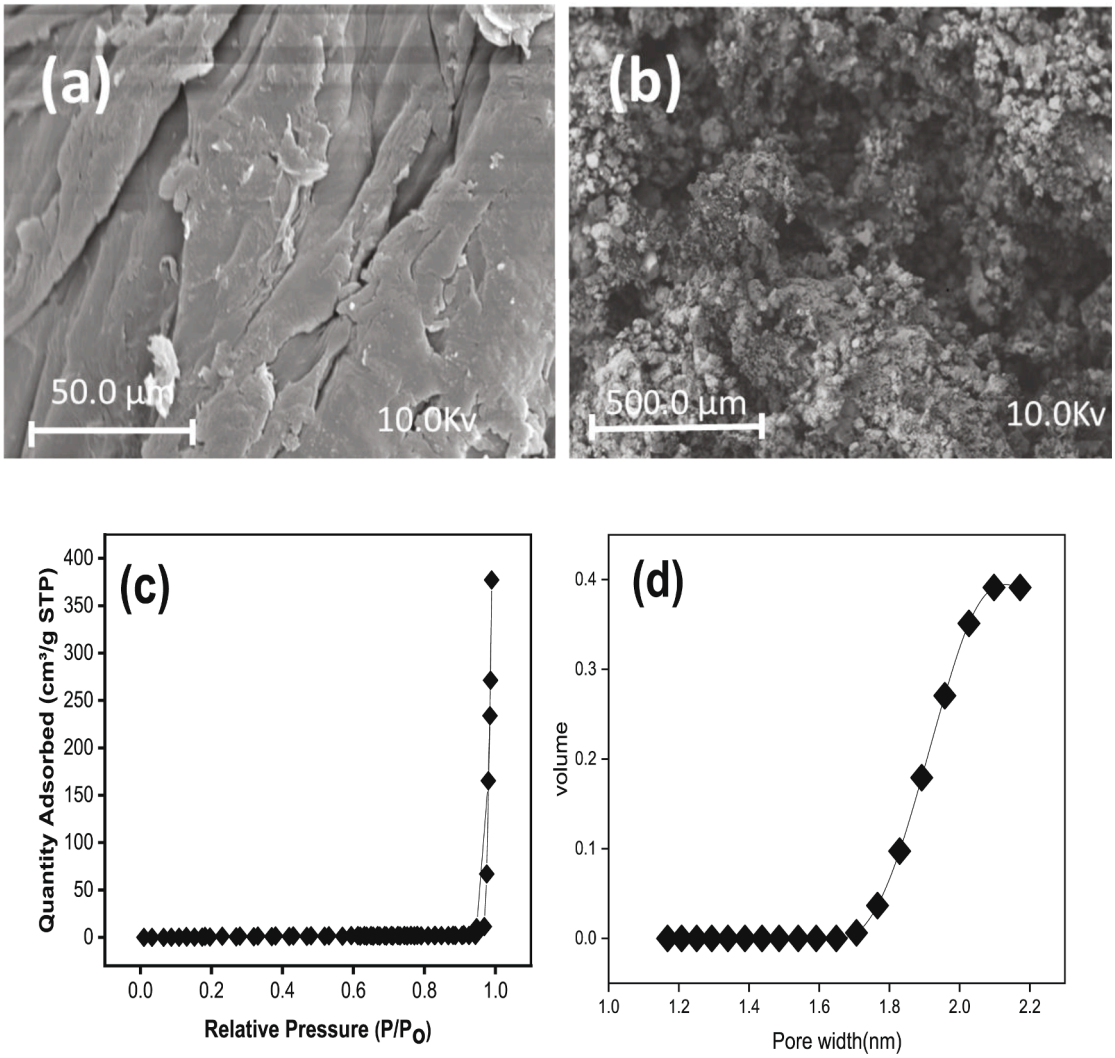

Fig. 1. SEM images (a) for chitosan (b) for CS-CI (c) N_2 adsorption and desorption isotherm for CS-CI. (d) pore size distribution; (e) XRD partner of CS-CI**;** TGA curves for (e) Chitosan (f) CS-CI; (g) Cu (II)-loaded CS-CI; (h) point of zero charge plot by the pH drift method.

where θ is the Bragg angle, λ represents the value of 1.540562 Å, and β in radians is the width broadening at half-peak height (WHPH). The estimated average particle size of the CS-CI was 68.60 nm, showing that the KIO_3 introduce in the chitosan material was well crystallized.

Fig. 1(f) shows the TGA of the CS-CI temperature behavior. The incorporated iodate has a considerable effect on the pyrolysis of CS-CI. The addition of iodate increase stability in the adsorbent, and the decomposition of the CS-CI shifted to relatively high temperatures. At temperatures above 650 °C, the release of volatiles was strongly hindered, with only a 70.4 % against 96.8 % loss. Furthermore, the maximum degradation state (304 –366 °C) resulted in 75.4 % weight loss without KIO_3, and weight loss of 11.35 % after the introduction of KIO_3 in the second stage of degradation.

The surface chemistry of the CS-CI and its interaction with Cu (II) was further examined by the FT-IR. The FT-IR of CS-CI and copper-laden CS-CI are shown in Fig. 1(g). The peak at 3624 cm^{-1} corresponds to OH stretching in –COOH group (Fu et al., 2018). The peaks at 1644, 2849 and 2930 cm^{-1} are assigned to C═O in COOH group, CH(V_{sy}) in (—CH_2 group), and CH(V_{as}) in (—CH_2 group [22], respectively. The peak at 1644 and 1548 is due to C—O stretching vibrations in NHCO [23] and the bending of N—H in NH_2, respectively. The peaks at 1072 and 657 cm^{-1} are related to —CO— groups and iodate compounds [16], respectively. After the sorption of Cu (II), the NH_2 and O—H stretching bands shows noticeable changes. It can be observed that 1664 cm^{-1} has shifted to a lower peak of 1631 cm^{-1}(Fig. 5b) related to N—H stretching under the influence of Cu (II) ions, while the band at 3624 cm^{-1} disappeared after formation of coordination bond between OH and Cu (II) (Cu-O). Besides, the peak at 1072 cm-1 (—CO—) is greatly reduced, which may be due to the formation of Cu (II)–CO-complex. The interaction of the iodate group with Cu (II) is also evident as the shift of the peak at 657 cm^{-1} to a higher peak at 847 cm^{-1} is observed. This verifies that the iodate, OH and NH groups on the CS-CI were the active sites for binding of Cu (II) ions.

The point of zero charge (pHp_{ZC}) is an important interfacial parameter in adsorbent characterization and is known to characterize the ionization behavior of surfaces [24]. Fig. 1(h) depicts a plot of estimated CS-CI pH_{PZC}, evidently showing the intersection at pH 4.8 (graph not shown). This indicates that there was a drift in the final equilibrium pH, and the net charge of the CS-CI was positive when pH values were below pH_{PZC} and negative at higher values of pH.

Cu (II) adsorption optimization study

Fig. 2(a) shows the effect of the amount of CS-Cl on the adsorption of Cu (II) from aqueous solution. Varying the amount of CS-SC from 0.1 to

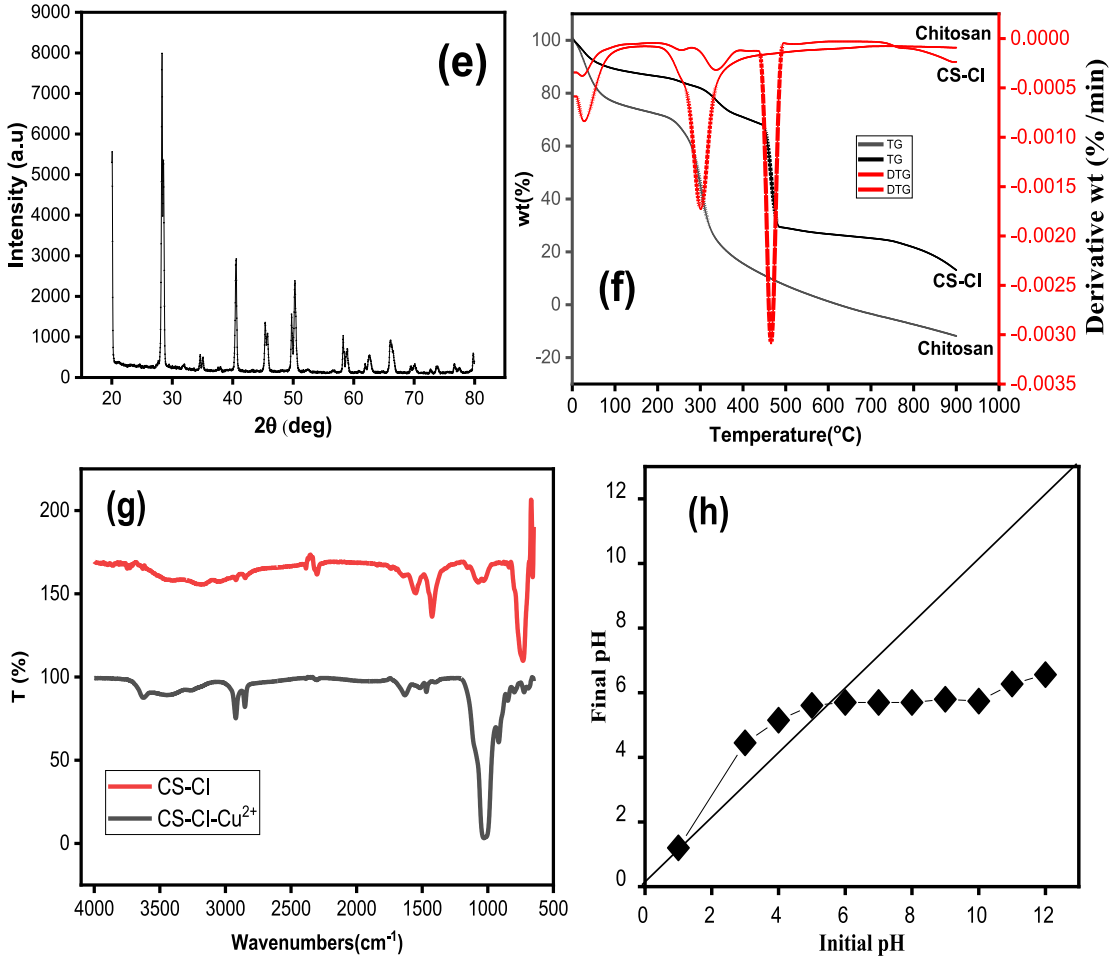

Fig. 1. (*continued*).

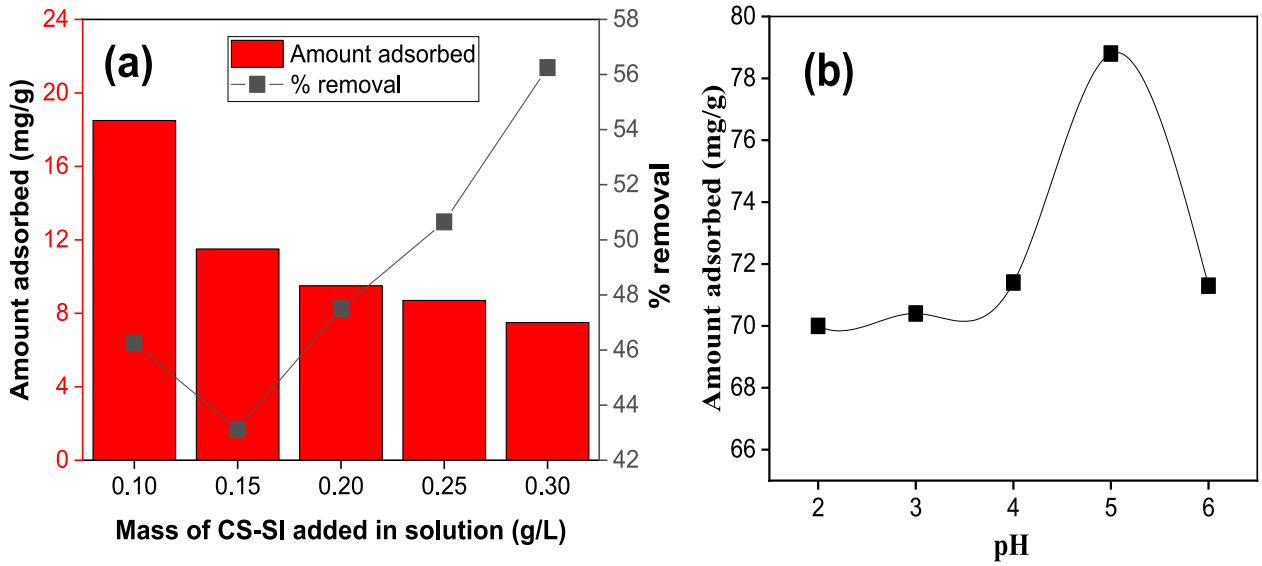

Fig. 2. (a) Effect of CS-CI dose on adsorption capacity (0.1 to 0.3 g / 200 mL, Cu concentration 20 mg/L) (b) Effects of initial solution pH (125 mg/L of Cu (II), dose 0.1 g).

3.0 g/L resulted in a decrease in the amount of Cu (II) adsorbed from 18.5 to 7.5 mg/g. This is due to the effective increase of adsorption sites with increasing CS-SC amount leading to an increase in adsorption capacity. As the adsorption progressed, a continuous increase in the dose resulted in a decrease in the ratio of Cu (II) concentration to SC-CI particles in the wastewater samples, causing a decrease in the binding

rate. Therefore, above adsorbent dosage of 0.1 mg/L, it is difficult to increase the adsorption capacity. To ensure reasonable adsorption capacity of CS-CI for Cu (II) and reduce cost, 0.1 g was considered as the optimal amount of CS-CI for all subsequent experiments.

Fig. 2 (b) shows Cu (II) adsorption on CS-CI under different pH(aq) conditions. Amount of Cu (II) adsorbed increased as the pH (aq)value increased. The uptake of Cu (II) occurs mainly through coordination with —NH_2 on CS-CI (Eq. (4)).

$$Cu^{2+} + nRNH_2 \leftrightarrow Cu(RNH_2)_n^{2+} \ by\ cordination \quad (4)$$

It is possible that two-OH group and one NH_2 group are grabbed by Cu^{2+} [25] or the NH_2 and the iodate act as a chelating sites for the Cu (II) [16]. As clearly demonstrated below (Fig. 2), the amount adsorbed (mg/g) decrease with further increase in pH (aq), with maximum amount of Cu (II) removal achieved at pH 5.i.e., most effective chemical interactions between Cu (II) and NH_2 and OH groups take place at pH 5. No substantial variation in efficiency of Cu (II) uptake by CS-CI at lower pH(aq) of 2–4. This is because the functional groups were protonated ($R-NH_3^+, R-OH_2^{2+}$) under strong acidic condition (2–4), which hinders their capacity to capture metal cations. But with the increase of pH (i.e., under relatively weak acidic conditions), the adsorption capacity of CS-CI is enhanced due to the binding of Cu (II) to more negative surfaces through electrostatic reactions, which is agreeing with high Cu (II) removal at higher pH of 5. In addition, this result is consistent with the surface properties of the adsorbent, as the measurements of the pH_{pzc} (isoelectric point), which defined the pH at which the net charge on the surface of the CS-CI is zero, revealed that the isoelectric point of the CS-CI was 4.8 (Fig. 1 h). Above the isoelectric point, the adsorbent surface is negatively charged (Eq. (5) and Eq. (6)), which shows more available sites for the adsorption of toxic Cu (II) in solution.

$$OH^- + R-NH_3^+ \rightarrow R-NH_2 + H_2O \quad (5)$$

$$OH^- + R-OH_2^{2+} \rightarrow R-HO^- + H_2O \quad (6)$$

The protonation of the NH_2 group (due to deprotonation of other functional groups like –OH) may explain the decrease in adsorption of Cu (II) at pH(aq) > 5. Moreover, protonation constant (log k_P) of NH_2 is about 6.2 (Wu et al., 2014), so more than 20 % of the amino groups are protonated even at pH 6 [25], leading to change in surface potential to positive (Eq. (7)). Elsewhere, it is reported that as low as pH 5, the NH_2 group of the chitosan is protonated [26].

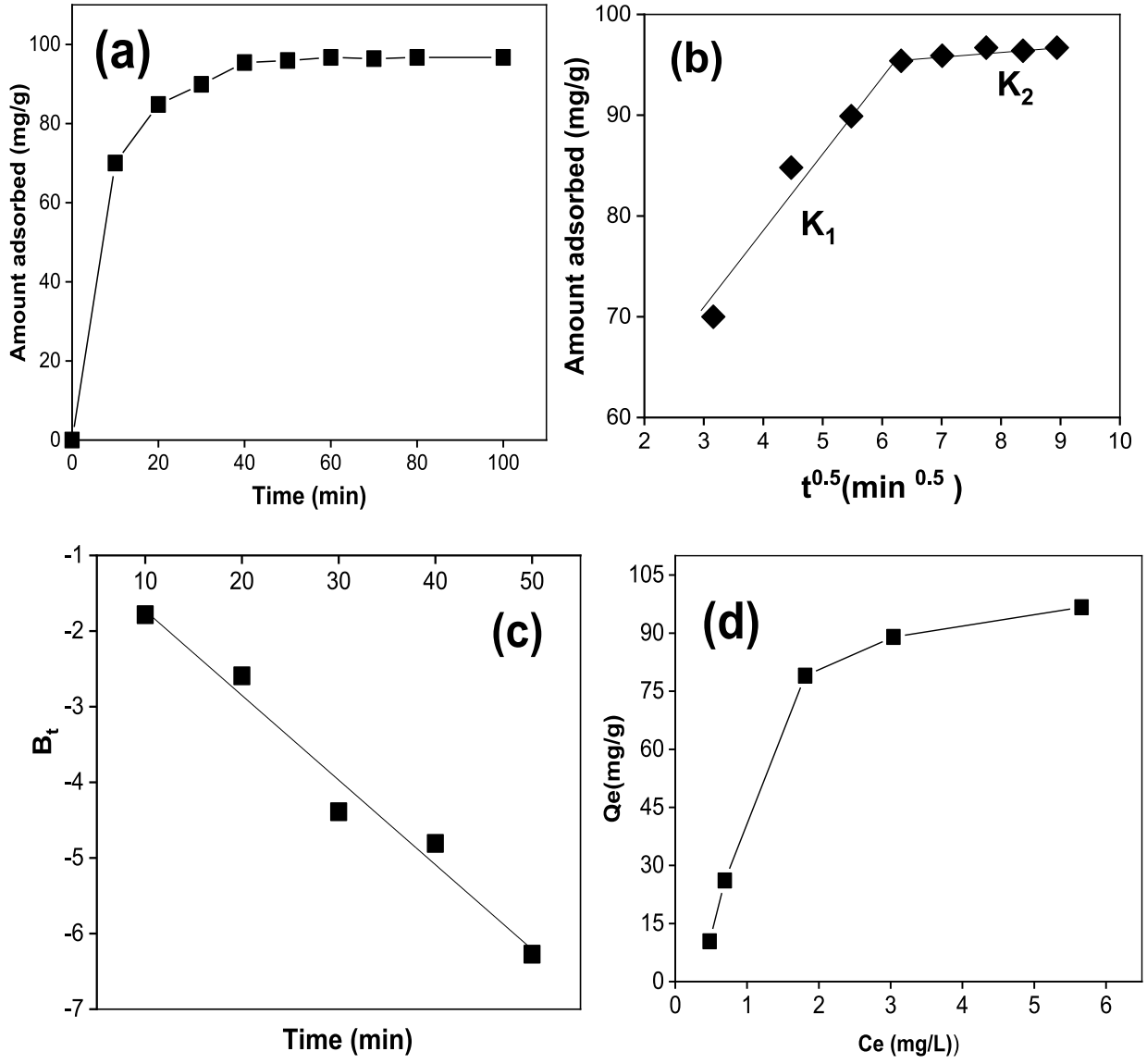

Fig. 3. (a) Sorption kinetic curve of Cu (II) ion by CS-CI (b) Weber-Morris plot, (c) Boyd kinetic plot (pH 5, dosage 0.1 g/ 200 mL, Cu $(II)_o$ = 125 mg/L; temperature = 25 °C; agitation rate = 250 rpm). (d) Isotherm curve of CS-CI adsorption for Cu (II) (0.1 g of CS-CI, pH 5.0; agitation speed 150 rpm; contact time 1 h.20 min).

$$H^+ + R-NH_2 \leftrightarrow R-NH_3^+ \quad (7)$$

The reactions of Eqs. (5)–(7) participate during the adsorption of Cu (II) on CS-CI, which may explain the increase or decrease of solution pH after adsorption. Additionally, in aquatic system, Cu existed primarily as free Cu (II) ion at pH values below 6.0, and as $Cu_2(OH)_2^{2+}$ (aq) or $CuOH^+$ (aq) at pH values above 6.0 [27]. It has been demonstrated during adsorption of Cu (II) on to adsorbents, there appear to be competition between ionic Cu (II)(radius 0.7A) and the hydrated Cu (II)(radius 4.19 A), with former easily adsorbed onto the pore of the adsorbent due to the smaller radius [28]. In this work, the pore size of CS-CI is 2.0 nm, so the competition is negligible, while the protonation of NH_2 may be the main factor. Flores-Alamo et al. [29] reported similar optimal for Cu (II) removal on modified chitosan material at pH 5. All subsequent experiments were conducted at pH value of 5. Besides, adsorption above pH 6 will result in an additional energy cost to overcome the repulsive force (Eq. (7)).

Kinetic and equilibrium adsorption isotherm

Adsorption of Cu (II) on CS-CI was fast at the initial 0–20 min as presented in Fig. 3a. This is because the concentration Cu (II) and number of active sites of the CS-CI were larger in the initial adsorption phase (0–20 min), and the large number of active sites on the CS-CI can bind Cu (II) ions. However, it can be seen that the adsorption capacity increases gradually and reaches equilibrium after 60 min. This is due to reduction in active sites on CS-CI, thus decreasing the possibility of Cu (II) chelation.

In addition, as the adsorption proceeds, the H^+ of the reactive functional group is released into solution, lowering the pH of the waste sample [30], thereby slowing down the binding of Cu (II) by CS-CI. Furthermore, at equilibrium, the adsorbent performance is a function of the adsorbent surface area and porosity [31]. The CS-CI has a good pore structure, and the Cu (II) may slowly migrate from the adsorbent surface into the pores at equilibrium by intraparticle diffusion. Furthermore, reaching equilibrium in such a short time highlights the application potential of CS-CI. This is in contrast with about 90 and 120 min exposure time reported for chitosan/carbon nanotubes [32], and with up to 12 days to reach equilibrium for chitosan particles [33]. As shown in Fig. 3(a), an exposure time of 60 min could be considered sufficient for the quantitative removal of Cu (II) by CS-CI, so subsequent experiments were performed at an exposure time of 70 min. The data from the batch adsorption experiments were fitted with pseudo-first-order (Eq. (8)) and second-order equations (Eq. (9)).

$$\ln(q_e - q_t) = \ln(q_e) - k_1 t \quad (8)$$

$$\frac{t}{q_t} = \frac{1}{k_2 q_e^2} + \frac{1}{q_e} t \quad (9)$$

where q_e and q_t are Cu (II) adsorption at equilibrium and time t. k_1(min-1) and k_2 (g.mg-1.min-1) correspond to the rate constants for the pseudo-first-order and pseudo-second-order equations, respectively.

Table 1 lists the kinetic parameters for Cu (II) adsorption. The discrepancies in the calculated and experimental Q_e values for the pseudo-first-order kinetic model, as well as the poor R^2 value, suggest that the model is not ideal for explaining the adsorption kinetic data. Therefore, a further fitting of the pseudo-second-order kinetic model to the adsorption data was initiated. The pseudo-second order R^2 (0.9998) gives the best fit in the data, so the values of $Qe_{(exp)}$ and $Qe_{(cal)}$ are in good agreement.

Kinetic data were further evaluated using an intraparticle diffusion model and a Boyd kinetic model that included information on the kinetic properties of the adsorption process. The intra-particle diffusion model is represented by the following equation (Eq. (10)).

$$q_t = k_c t^{1/2} + C \quad (10)$$

where C is the intercept and kc are the intraparticle diffusion rate constant representing the gradient of the linear portion of the curve. The intraparticle model is sole rate-limiting step if the plot the Q_t versus $t^{1/2}$ a passing through the origin, while large intercept explains a process controlled by surface or boundary layer adsorption [34]. According to the intraparticle plot model, the co-occurrence of two linear diffusional region (with constants K_1 & K_2) that did not start via the origin of the graph was observed, indicating that intraparticle diffusion is not the only rate limiting step for the adsorption of Cu (II) ion. These two distinct regions are due to the simultaneous adsorption of Cu (II) by CS-CI, sequentially via surface adsorption and intraparticle diffusion. For example, the first linear diffusion region is the boundary layer effect (external mass transfer process), where Cu (II) ions are transported through the solution phase to the CS-CI surface. The second linear diffusion region is dominated by intra-particle diffusion processes (i.e., adsorption of Cu (II) inside the CS-CI particles). The gradients have very different diffusion rate constants (k) and the second region is significantly smaller. This difference may be due to the bimodal pore character [35] of the CS-CI particles, where the first region accounts for macropore diffusion and the second region accounts for micropore diffusion. The results show that the diffusion rate in the microporous region becomes significantly slower. This is because the diffusing molecules become comparable to the pore size and the collision with the pore wall is a common phenomenon [35]. All evaluated constants, parameters, and R^2 values are listed in Table 1.

To determine the slowest step (external or internal diffusion) of Cu (II) adsorption in solution, the Boyd diffusion model is further expressed as follows (Eq. (11)):

$$B_t = -0.4977 - In(1 - \frac{q_t}{q_e}) \quad (11)$$

q_t and q_e represent the amount of Cu (II) ions adsorbed at time t and at equilibrium (infinite time). The Boyd model assumes that if a liner plot did not intercept the origin, particle diffusion is the rate limiting step, however, external mass transfer controlled the overall rate of adsorption process if linear plot is with intercept [24]. Bt value were plotted against the t as shown in Fig. 3(c), the Boyed kinetic plot was liner but did not pass via origin indicating that the adsorption of Cu (II) on to CS-CI was predominantly controlled by surface adsorption or chemical reactions [24]. The effective diffusion coefficient (Di) of Cu (II) into the CS-CI was obtained from Eq. (12).

Table 1
Parameters of adsorption kinetics and intraparticle-diffusion model for Cu (II) adsorption by CS-CI.

Pseudo-first-order kinetic model				Pseudo-second-order kinetic model			
Qe_{exp} (mg/g)	$Q_{e\ cal}$ (mg/g)	K_1 (min-1)	R_2	Q_e cal (mg/g)	K_2(g/mg.min)		R^2
96.7	39.5	0.030	0.8209	97.08	0.053		0.9998
Intrapaticle-diffusion model				**Boyd model**			
K1 (mg.(g. min0.5)$^{-1}$	**R_2**	**K_2 (mg.(g.min0.5)$^{-1}$**	**R2**	**Di × 10^{-13} (m^3/s)**	**B min^{-1}**	***K***	**R^2**
7.881	0.9663	0.479	0.7905	1.352	0.6117	0.1119	0.9745

$$B = \frac{\pi^2 D_i}{r^2} \tag{12}$$

where r is the radius of the CS-CI presumed to be spherical and B is the rate constant. The diffusion rate constant (B) obtained from the slop and R^2 of the plot are presented in Table 1. The value of Di indicated diffusion resistance in the pore volume transpired [36].

To analyze the equilibrium adsorption data, two different adsorption models were applied, including Langmuir (Eq. (13)) and Freundlich (Eq. (14)) [37,38]. The relation of Cu (II) uptake(qe) and Cu (II) equilibrium concentration (C_e) curve and isotherm parameters are shown in Fig. 3d and Table 2, respectively. The estimated parameters and R^2 values show that the Langmuir model describes the best fit to the equilibrium data ($R^2 = 0.9821$). The separation factor of the Langmuir isotherm model, which expresses the nature and character of the adsorption and predicts the feasibility [39], was also estimated. The estimated value of RL was 0.142, indicating the feasibility of CS-CI for Cu (II) adsorption. At 25 ± 0.5 °C and initial Cu (II) concentration (10–125 mg/L), the estimated maximum adsorption capacity reached 95.2 mg/g. The estimated maximum Cu (II) absorption capacity and equilibration time of CS-CI were compared with other chitosan-based absorbers found in the literature (Table 3a). Compared with most adsorbents, CS-CI showed encouraging removal performance, moreover, CS-CI showed faster Cu (II) uptake, reaching more than 80 % efficiency in 1.0 h, faster than other adsorbents.

$$\frac{C_e}{q_e} = \frac{1}{Q_m b} + \left(\frac{1}{Q_m}\right) C_e \tag{13}$$

$$\mathrm{In}q_e = \mathrm{In}k_\mathrm{F} + \frac{1}{n}\mathrm{InC_e} \tag{14}$$

where Q_m is the adsorption capacity (mg/g) and b is the equilibrium bond energy. K_F and n are Freundlich constants that define the relative retention affinity of Cu (II) and the strength and extent of disproportionation on the adsorbent, respectively, and C_o and C_e are the initial and equilibrium concentrations (mg/g), respectively.

Thermodynamic parameters and activation energy

The driving force for adsorption chemical reaction is the Gibbs free energy of reaction (ΔG^o) that, involve an enthalpy (ΔH^o), and entropy (ΔS^o) contribution. Table 3b summarized the computed thermodynamic parameters of the system (i.e. ΔG^o, ΔH^o and ΔS^o), which were obtained by using the following equations (Eqs. (15) and (16)):

$$\Delta \mathrm{G}^o = -\mathrm{RTln}K_\mathrm{C} \tag{15}$$

ΔH^o and ΔS^o were calculated from Vant Hoff's equation, shown below

$$\mathrm{In}\left(\frac{\mathrm{qe}}{\mathrm{Ce}}\right) = \left(\frac{\Delta S}{R}\right) - \left(\frac{\Delta H}{R}\right)\frac{1}{T} \tag{16}$$

where K_C is the equilibrium constant, q_e is the amount of adsorbate on the adsorbent per liter of the solution at equilibrium (mg L^{-1}), C_e is the equilibrium concentration of adsorbate in the solution (mg L^{-1}) and C_o and C_e are the initial and equilibrium concentration of the Cu (II) ions in solution, respectively. R is the universal gas constant (8.314 J. mol^{-1}. K^{-1}).

Table 2
Adsorption isotherm parameters for Cu (II) adsorption by CS-CI.

Langmuir Model				Freundlich Model		
Q_m(mg/g)	b (L/mg)	R_L	R^2	1/n	K_F (mg/g)(L/mg)^n	R^2
95.2	0.048	0.142	0.9737	1.256	1.279	0.6565

Table 3a
Comparison of adsorption capacities for different adsorbents.

Absorbent	Qm mg/g.	Equilibrium Time (h)	Reference
CS-CI	95.2	1	This study
Dromaius novaehollandiae eggshell and chitosan composite	48.30	1	[40]
Chitosan/clay/magnetite composite	17.20	2	[41]
Chitosan immobilized on bentonite,	21.55	4	[42]
Chitosan-8-HydroxyquinolineBeads	52.90	4	[43]
Chitosan/*Sargassum sp*	1.08	6	[44]
Low cost magnetic adsorbent	22.41		[45]
Carbon mineral nanocomposite	50.66	7	[46]

Table 3b
Thermodynamic parameters for the adsorption of Cu (II) at various temperatures.

Temp (K)	InK	ΔG^o kJ/ mol	ΔS^o kJ/ mol k	ΔH^o kJ/ mol
25	0.4885	−1.904	0.15	43.47
30	0.9690	−2.825		
40	1.4024	−4.228		

As shown in Fig. 4a, the adsorption of Cu (II) increased with increasing temperature, confirming the fact that chemisorption occurs between Cu (II) ions and CS-CI [47]. As the temperature increases, ionic interactions between Cu (II) and the negative sites on the amine and iodate are strongly supported. The adsorption percentage of Cu (II) increased by 8.42 % as the temperature increased from 25 °C to 40 °C.

The calculated ΔG^o values became more negative (from −1.904 to −4.228 kJ/mol) as the temperature increased, indicating an increase in the spontaneity and feasibility of Cu (II) adsorption at higher temperatures. The calculated ΔH^o was positive (43.47 kJ/mol), which indicates adsorption process was endothermic. The observed endothermic behavior may be related to more than just formation of coordination bonds with Cu (II). Moreover, surface amine groups hydrogen-bonded to hydroxyl groups are released, thus requiring energy (Scheme 1(a–b)). Furthermore, the adsorbent is porous and the adsorption sites are also in the pores, therefore, the observed endothermic behavior may also be due to endothermic processes, including diffusion resistance [48]. All the afformation processes combined to give a positive enthalpy, the sum of which is greater than the negative ethalpy of formation of the copper–amine complex [48].

The positive entropy change ΔS^o (0.15 kJ/mol K) is consistent with a favorable adsorption process. Positive entropy values are generally associated with the expulsion of solvent originally present in the cation coordination sphere or the displacement of hydrogen-bonded amine groups into the medium [48], therefore, the degree of dissociation and randomness in the adsorption process at the Cu (II)/CS-CI interface is increased [28] and increased entropy.

To estimate the adsorption type (physical or chemical), magnitude of activation energy was assessed at three different temperatures (25 to 40 °C). The activation energy allows estimation of the energy barrier that metal ions need to overcome before chelating the adsorption site. The activation energy for Cu (II) adsorption onto CS-CI, was expressed through the modified Arrhenius equation [49] as demonstrated in Eq. (17).

$$\mathrm{In}\,S^* = In(1-\theta) - (E_a/R)\frac{1}{T} \tag{17}$$

where θ is the surface coating, S^* is the sticking probability, and E_a (kJ/mol) is the activation energy.

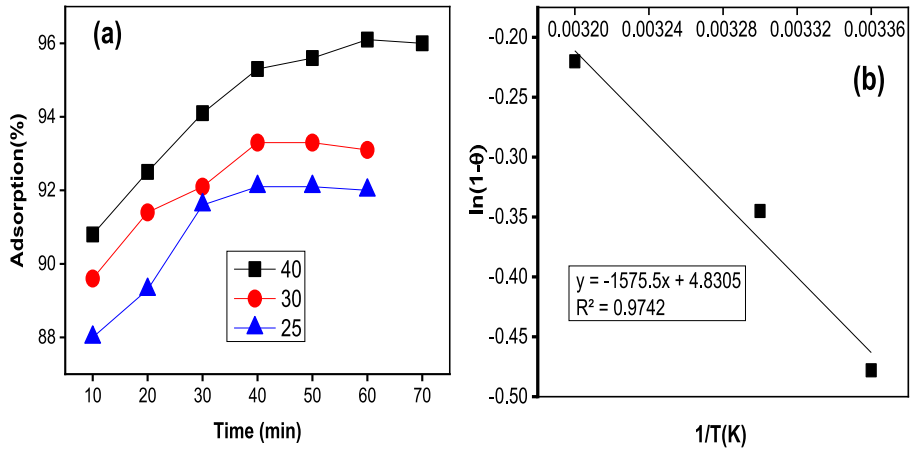

Fig. 4. Effect of temperature on the adsorption capacity of Cu (II) (pH 5, dosage 0.1 g/ 200 mL, Cu concentration 125 mg/L) Plot of Ln(1-θ) versus 1/T for adsorption of Cu (II) onto CS-CI.

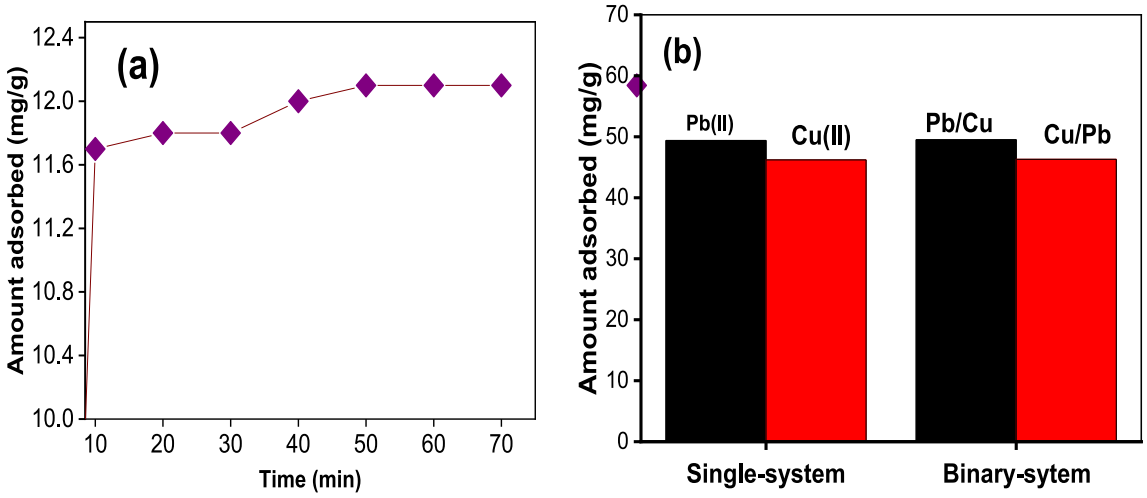

Fig. 5. (a) Wastewater treatment of Cu (II) using CS-CS(70 min, 0.1 g, optimum pH). (b) single–solute and multi-solute using CS-CI (0.1 g, 75 mg/L, 200 rpm, optimum pH.

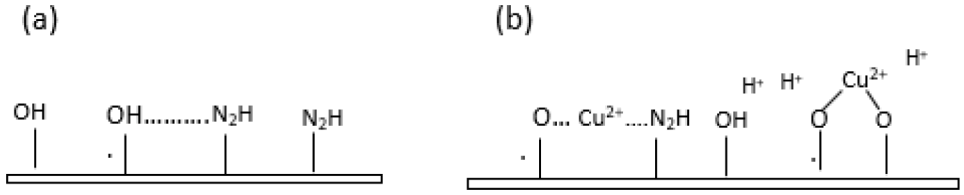

Scheme 1. Proposed mechanism of copper adsorption on CS-CI during release of the amine groups.

$$\theta = \left[1 - \frac{q_e}{C_e}\right] \tag{18}$$

Value of E_a was obtained from $-E_a/R$ (slop) by plotting In(1-θ) against 1/T.

The value of E_a obtained from Fig. 4b was positive, corroborating the endothermic adsorption behaviour. Usually physisorption processes are reversible, have small energy requirements (<8.4 kj/mole), and equilibrium is easily reached, while chemisorption processes are specific, involve greater forces, and thus require greater activation energy (at 8.4 Kj/mol-80 Kj/mol) [49]. Our present work shows that *Ea* is on the order of 13.10 Kj/mol, indicating that chemisorption is the main process of adsorption.

Probable mechanism of adsorption of Cu (II) onto CS-CI

The mechanism of adsorption process can be explained through combined mechanisms. Different functional groups and pores of the CS-CI can facilitate the removal of Cu (II) through complexation reactions, electrostatic attraction and intraparticle diffusion mechanism. The main mechanisms for Cu (II) adsorption can be summarized as follows [22,48]:

(1) Formation of coordination bonds with metal ions via chelating effects

$$\equiv -\mathrm{OH} + \mathrm{Cu}^{2+} + \equiv -\mathrm{OH} \leftrightarrow \equiv -\mathrm{OH}\cdots\mathrm{Cu}^{2+}\cdots\mathrm{HO} - \equiv$$

$$\equiv -NH_2 + Cu^{2+} + \equiv -NH_2 \leftrightarrow \equiv -NH_2\cdots Cu^{2+}\cdots H_2N - \equiv$$

$$\equiv -OH + Cu^{2+} + \equiv -NH_2 \leftrightarrow \equiv -OH\cdots Cu^{2+}\cdots H_2N - \equiv$$

(2) Intraparticle diffusion phenomenon and electrostatic attraction

Furthermore, when the surface active sites of I-IC slowly reached equilibrium state, Cu (II) ions might migrate from the surface of I-IC to the pores through intraparticle diffusion, which is a possible phenomenon in porous materials. The Cu (II) is then adsorbed by surface hydroxyl (—OH) groups and iodate anion (IO_3^-), forming (—O $-Cu^{2+}-$ O-) bridging spaces and ($-IO_3^- -Cu^{2+} -IO_3^-$-) bridging species according to the following [22]:

$$\equiv -O^- + Cu^{2+} + \equiv -O^- \rightarrow \equiv -O-Cu^{2+}-O- \equiv$$

$$\equiv -NH_3^+IO_3^- + Cu^{2+} + \equiv -NH_3^+IO_3^- \rightarrow$$
$$\equiv -NH_3^+IO_3^- - Cu^{2+} - IO_3^-NH_3^+ - \equiv$$

$\equiv$ = surface of adsorbent.

The synthesis of CS-CI and probable interaction of Cu (II) with the CS-CI is schematically illustrated in scheme 2.

Competitive adsorption and treatment of industrial wastewater

Wastewater contains too many metals that may hinder their removal or have little effect on the sorbent's ability to remove metals. Thus, co-ion sorption data play an important role in the design and implementation of wastewater treatment system [50], which is vital for robust water treatment system. Therefore, bimetallic tests involving Pb(II) and Cu (II) were performed by batch equilibrium experiments using 75 mg/L of each metal. 200 mL of the bimetallic blend were added to the flasks containing 0.1 g/L CS-Cl and equilibrated in a shaking bath (70 min /150 rpm). It was observed that CS-CI simultaneously removed Cu (II) and Pb(II) in the co-ion system (Fig. 5(b)). The presence of competing cations has no effect on the existing binding sites, as the same amount of adsorbed metal was recorded in co-adsorption studies. This is because the metals either bind to many other active sites available on the sorbent, or the sorbent has a large number of binding sites so competition is negligible[51].

After industrial effluent wastewater is treated and discharged, the water quality may not reach acceptable limits due to residual heavy metals. In addition, the chemical composition of industrial wastewater can be quite different from stimulated wastewater due to some differences in solution chemistry caused by multiple underlying factors present in actual wastewater (e.g., co-existing ions, pH, etc.). Consequently, CS-CI adsorbent was used in experiment involving real industry wastewater to see if the water quality could be improved or the underlying factors might hinder adsorption efficiency CS-CI. The wastewater sample was analyzed for initial concentration of Cu (II) and pH before treatment and found to be 2.0 mg/L and 1.0, discretely. The result (Fig. 5a) showed that CS-CI was able to remove Cu (II) to levels below 0.087 mg/g (96 %). Regardless of whether the metal ion composition of the real wastewater samples is more multipart, the results indicate that CS-CI has application potential for the removal of Cu (II) in industrial wastewater.

Challenges and future prospects

Chitosan has a wide range of potential applications, from wastewater and cosmetic products to biomedicine. Though chitosan-based adsorbents have a spectrum of applications, researchers have faced different challenges from the adsorptive removal of pollutants including heavy metals by the chitosan-based adsorbents especially the leaching and lower chemical and physical stability, high pH sensitivity, low surface area and porosity and solubility in most organic acids. To overcome these challenges and tailor chitosan-based adsorbents to desired properties and specific applications, researchers have attempted to modify them through physical and chemical processes. Continuous mode adsorption is more relevant to the development of commercial adsorbents and the practical application of adsorbents, so it is of great

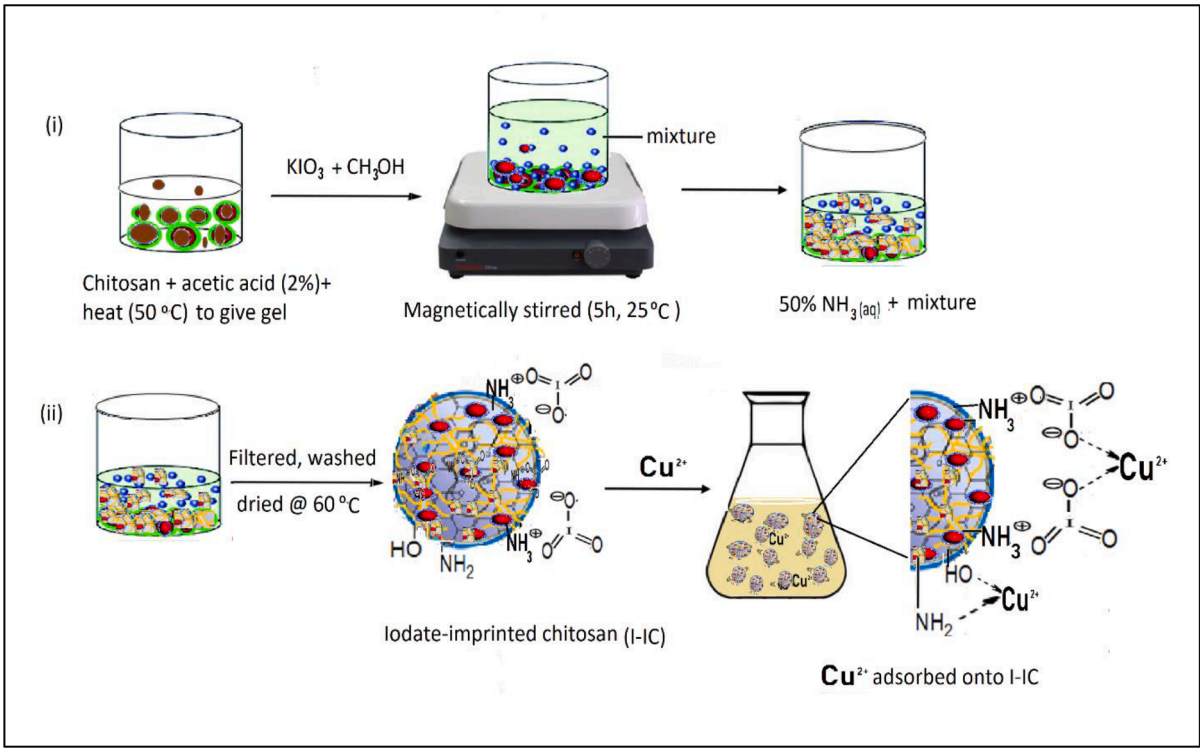

Scheme 2. Schematic illustration for the synthesis of CS-CI and probable interaction of Cu (II) with CS-CI.

significance to study and develop adsorption columns for chitosan-based adsorbents.

Conclusion

The CS-CI composite with high surface area, high thermal stability with efficient and fast approach to Cu (II) removal has been fabricated. The CS-CI which was prepared via media exhibited high adsorption toward the metal ions and is relatively stable and can withstand faily high temperatures.

The adsorption was pH dependent and the highest capacity for adsorption (78. 8 mg/g) was obtained at pH 5. More importantly, the adsorbent showed good ability in adsorbing Cu (II) in industrial effluents. Interestingly, CS-CI did not show selectivity for removal of binary metals in competitive studies, a promising property for the removal of a wide range of pollutants in wastewater. The kinetic adsorption reactions suggest that adsorption process is mainly controlled by chemisorption, with pore diffusion contributing to the mass transfer phenomenon. The adsorption mechanism was expected to take place through electrostatic attraction or chelation. The CS-CI prepared from low-cost materials in this study has a high potential for Cu (II) remediation in aqueous environments, making it attractive both environmentally and economically.

CRediT authorship contribution statement

Aloysius Akaangee Pam: Formal analysis, Writing – original draft, Investigation, Supervision, Conceptualization. **Olugbenga Oluseun Elemile:** . **Dallatu Ephraim Musa:** Writing – original draft, Investigation. **Maureen Chijoke Okere:** Validation, Writing – review & editing. **Amos Olusegun:** Validation, Writing – review & editing. **Yakubu Ahmed Ameh:** Investigation, Writing – review & editing.

Declaration of Competing Interest

The authors declare that they have no known competing financial interests or personal relationships that could have appeared to influence the work reported in this paper.

References

[1] A. Sharma, M. Singh, K. Arora, P.P. Singh, R. Badru, T. Singh Kang, S. Kaushal, Preparation of cellulose acetate-Sn(IV) iodophosphate nanocomposite for efficient and selective removal of Hg2+ and Mn2+ ions from aqueous solution, Environ. Nanotechnol. Monit. Manage. 16 (2021) 100478, https://doi.org/10.1016/j.enmm.2021.100478.

[2] Y. Cen, Y. Li, H. Deng, H. Ding, S. Tang, X. Yu, F. Xu, Z. Zhu, Removal of Copper (II) from Aqueous Solution by a Hierarchical Porous Hydroxylapatite-Biochar Composite Prepared with Sugarcane Top Internode Biotemplate, Water. 14 (2022) 1-20, ijms-23-02396-v2.

[3] L.i. Zhou, Y. Huang, W. Qiu, Z. Sun, Z. Liu, Z. Song, Adsorption Properties of Nano-MnO2–Biochar Composites for Copper in Aqueous Solution, Molecules 22 (1) (2017) 173.

[4] C. Daniele, S. Alves, B. Healy, L.A.D.A. Pinto, T.R. Sant, A. Cadaval, C.B. Breslin, Recent Developments in Chitosan-Based Adsorbents for the Removal of Pollutants from Aqueous Environments, Molecules 26 (2021) 1–45.

[5] Z. Wang, X. Luo, Z. Song, K. Lu, S. Zhu, Y. Yang, Y. Zhang, W. Fang, J. Jin, Microporous polymer adsorptive membranes with high processing capacity for molecular separation, Nat. Commun. 13 (2022) 1–10, https://doi.org/10.1038/s41467-022-31575-y.

[6] A. Wołowicz, Z. Hubicki, Enhanced removal of copper(II) from acidic streams using functional resins: batch and column studies, J. Mater. Sci. 55 (2020) 13687–13715, https://doi.org/10.1007/s10853-020-04982-z.

[7] D.M. Smith, B. Hamwi, R.E. Rogers, Carbon nanomaterial-based aerogels for improved removal of copper(ii), zinc(ii), and lead(ii) ions from water, Environ. Sci. Adv. 1 (2022) 208–215, https://doi.org/10.1039/d2va00049k.

[8] A.W. Knight, A.B. Tigges, A.G. Ilgen, Adsorption of copper (II) on mesoporous silica: The effect of nano-scale confinement, Geochem. Trans. 19 (2018) 1–13, https://doi.org/10.1186/s12932-018-0057-4.

[9] J. Li, M. Li, Q. Song, S. Wang, X. Cui, F. Liu, X. Liu, Efficient recovery of Cu (II) by LTA-zeolites with hierarchical pores and their resource utilization in electrochemical denitrification: Environmentally friendly design and reutilization of waste in water, J. Hazard. Mater. 394 (2020), 122554, https://doi.org/10.1016/j.jhazmat.2020.122554.

[10] Z. Zou, Z. Shi, L. Deng, Highly efficient removal of Cu (II) from aqueoussolution using a novel magnetic EDTA functionalized CoFe2O4, RSC Adv. 7 (2017) 5195–5205, https://doi.org/10.1039/C6RA26821H.

[11] B. Zhang, S. Wang, L. Fu, L. Zhang, Synthesis and Evaluation of 8-Aminoquinoline-Grafted Poly (glycidyl methacrylate) for the Recovery of Pd (II) from Highly Acidic Aqueous Solutions, Polymers (Basel). 10 (4) (2018) 437.

[12] R.K. Ramakrishnan, V.V.T. Padil, M. Cern, R.S. Varma, Eco-Friendly and Economic , Adsorptive Removal of Cationic, (2021) 1–21.

[13] D. Avcı, S. Altürk, F. Sönmez, Ö. Tamer, A. Başoğlu, Y. Atalay, B.Z. Kurt, N. Dege, Three novel Cu (II), Cd(II) and Cr(III) complexes of 6−Methylpyridine−2−carboxylic acid with thiocyanate: Synthesis, crystal structures, DFT calculations, molecular docking and α-Glucosidase inhibition studies, Tetrahedron 74 (2018) 7198–7208, https://doi.org/10.1016/j.tet.2018.10.054.

[14] N.A.A. Qasem, R.H. Mohammed, Removal of heavy metal ions from wastewater : a comprehensive and critical review, Clean Water. 36 (2021) 1–15, https://doi.org/10.1038/s41545-021-00127-0.

[15] Q.X. Wu, D.Q. Lin, S.J. Yao, Design of chitosan and its water soluble derivatives-based drug carriers with polyelectrolyte complexes, Mar. Drugs 12 (2014) 6236–6253, https://doi.org/10.3390/md12126236.

[16] A.H. Gedam, R.S. Dongre, Adsorption characterization of Pb(ii) ions onto iodate doped chitosan composite: equilibrium and kinetic studies, RSC Adv. 5 (2015) 54188–54201, https://doi.org/10.1039/c5ra09899h.

[17] A.A. Pam, A.H. Abdullah, Physicochemical properties of porous activated carbon prepared from palm kernel shell through a low-cost activation protocol, 118 (2022) 1–7.

[18] A.A. Adeyi, M.C. Uzoukwu, L.T. Popoola, A.S. Yusuff, E. Bernard, A.A. Pam, A. T. Ogunyemi, A. Hamisu, Equilibrium and Kinetic Analysis on Cadmium Ion Sequestration from Aqueous Environment by Impregnated Chicken Feather Alkaline Biosorbent, Int. J. Eng. Res. Africa. 60 (2022) 15–28, https://doi.org/10.4028/p-734lko.

[19] A. Rohaizad, Z. Adlan, M. Hir, U. Abdul, A. Mustafa, Z. Aspanut, A. Akaangee, Biosynthesis of silver nanoparticles using Allium sativum extract assisted by solar irradiation in a composite with graphene oxide as potent adsorbents, Results Chem. 5 (2023), 100731, https://doi.org/10.1016/j.rechem.2022.100731.

[20] A.L. Cazetta, O. Pezoti, K.C. Bedin, T.L. Silva, A. Paesano Junior, T. Asefa, V. C. Almeida, Magnetic Activated Carbon Derived from Biomass Waste by Concurrent Synthesis: Efficient Adsorbent for Toxic Dyes, ACS Sustain, Chem. Eng. 4 (2016) 1058–1068, https://doi.org/10.1021/acssuschemeng.5b01141.

[21] G. Nagaraju, H. Nagabhushana, R.B. Basavaraj, G.K. Raghu, D. Suresh, H. Rajanaika, S.C. Sharma, Green , non chemical route for the synthesis of ZnO superstructures , Evaluation of its applications towards Green , non-chemical route for the synthesis of ZnO superstructures , Evaluation of its applications towards Photocatalysis , Photoluminescence an, (2016), doi:10.1021/acs.cgd.6b00936.

[22] Y. Fu, Y. Huang, J. Hu, Preparation of chitosan / MCM-41-PAA nanocomposites and the adsorption behaviour of Hg (II) ions, R. Soc. Open Sci. 5 (3) (2018) 171927.

[23] D.C. and P.L. Lingkai Zhu, Yuyuan Yao, The e ff ective removal of Pb 2 + by activated carbon fi bers modi fi ed by L -cysteine: exploration of kinetics , thermodynamics and mechanism, RSC Adv. (2022) 20062–20073, doi:10.1039/D2RA01521H.

[24] Y.C.S. Prabhat Kumar Singha, Sushmita Banerjeeb, Arun Lal Srivastavac, Kinetic and equilibrium modeling for removal of nitrate from aqueous solutions and drinking water by a potential adsorbent, hydrous bismuth oxide, 2015, doi:10.5004/dwt.2010.1175.

[25] R. Juang, H. Shao, Effect of pH on Competitive Adsorption of Cu (II), Ni (II), and Zn (II) from Water onto Chitosan Beads, Adsorption 8 (2002) 71–78.

[26] R. Rabelo, R. Vieira, F. Luna, E. Guibal, M. Beppu, Adsorption of copper(II) and mercury(II) ions onto chemically-modified chitosan membranes: Equilibrium and kinetic properties, Adsorpt. Sci. Technol. 30 (2012) 1–21, https://doi.org/10.1260/0263-6174.30.1.1.

[27] X. Zuo, Preparation and Evaluation of Novel Thiourea / Chitosan Composite Beads for Copper (II) Removal in Aqueous Solutions, Ind. Eng. Chem. Res. 53 (2014) 1249–1255, https://doi.org/10.1021/ie4036059.

[28] B. Oladipo, E. Govender-opitz, T. V Ojumu, Kinetics , Thermodynamics , and Mechanism of Cu (II) Ion Sorption by Biogenic Iron Precipitate: Using the Lens of Wastewater Treatment to Diagnose a Typical Biohydrometallurgical Problem, (2021), doi:10.1021/acsomega.1c03855.

[29] N. Flores-Alamo, R.M. Gómez-Espinosa, M. Solache-Ríos, J.L. García-Rivas, R. E. Zavala-Arce, B. García-Gaitán, Adsorption behaviour of copper onto a novel modified chitosan material: thermodynamic study, Desalin. Water Treat. 57 (52) (2016) 25080–25088.

[30] L. Li, L. Zhao, J. Ma, Y. Tian, Y. Tian, Preparation of graphene oxide/chitosan complex and its adsorption properties for heavy metal ions, Green Process. Synth, 9 (2020) 294–303, https://doi.org/10.1515/gps-2020-0030.

[31] M.I. Khan, T.K. Min, K. Azizli, S. Sufian, H. Ullah, Z. Man, Effective removal of methylene blue from water using phosphoric acid based geopolymers: Synthesis, characterizations and adsorption studies, RSC Adv. 5 (2015) 61410–61420, https://doi.org/10.1039/c5ra08255b.

[32] S.R. Popuri, R. Frederick, C. ChiaYuan, F. ShingShyong, W. ChengChien, L. LienChieh, Removal of copper (II) ions from aqueous solutions onto chitosan/carbon nanotubes composite sorbent, Desalin. Water Treat. 52 (2014) 691–701, https://doi.org/10.1080/19443994.2013.826779.

[33] J.C.Y. Ng, W.H. Cheung, G. McKay, Equilibrium studies of the sorption of Cu (II) ions onto chitosan, J. Colloid Interface Sci. 255 (2002) 64–74, https://doi.org/10.1006/jcis.2002.8664.

[34] S. Bhowmik, V. Chakraborty, P. Das, Batch adsorption of indigo carmine on activated carbon prepared from sawdust: A comparative study and optimization of operating conditions using Response Surface Methodology, Results Surf. Interfaces. 3 (2021), 100011, https://doi.org/10.1016/j.rsurfi.2021.100011.
[35] Q. Zhu, G.D. Moggridge, C. D'Agostino, Adsorption of pyridine from aqueous solutions by polymeric adsorbents MN 200 and MN 500. Part 2: Kinetics and diffusion analysis, Chem. Eng. J. 306 (2016) 1223–1233, https://doi.org/10.1016/j.cej.2016.07.087.
[36] M. Maslova, V. Ivanenko, P. Evstropova, N. Mudruk, L. Gerasimova, Investigation on Purification of Saturated LiNO 3 Solution Using Titanium Phosphate Ion Exchanger : Kinetics Study, Int. J. Mol. Sci. 23 (2022).
[37] A.A. Muhammad, U.F. Audu, A.S. Onakpa, A.A. Pam, Thermodynamic Study of the Competitive Adsorption of Chromium (III) Ions and Halides onto Sweet Orange (Citrus Sinensis) Peels as Adsorbent, J. Environ. Anal. Chem. 01 (2014) 1–7, https://doi.org/10.4172/jreac.1000114.
[38] F.A. Ugbe, A.A. Pam, A.V. Ikudayisi, Thermodynamic Properties of Chromium (III) Ion Adsorption by Sweet Orange (Citrus sinensis) Peels, Am. J. Anal. Chem. 05 (2014) 666–673, https://doi.org/10.4236/ajac.2014.510074.
[39] D. Datta, H. Uslu, Adsorptive Separation of Lead (Pb 2+) from Aqueous Solution Using Tri- n -octylamine Supported Montmorillonite, J. Chem. Eng. Data 62 (1) (2017) 370–375, https://doi.org/10.1021/acs.jced.6b00716.
[40] R.K. Anantha, S. Kota, An evaluation of the major factors influencing the removal of copper ions using the egg shell (Dromaius novaehollandiae): chitosan (Agaricus bisporus) composite, 3 Biotech. (2016) 61–116, https://doi.org/10.1007/s13205-016-0381-2.
[41] D.W. Cho, B.H. Jeon, C.M. Chon, Y. Kim, F.W. Schwartz, E.S. Lee, H. Song, A novel chitosan/clay/magnetite composite for adsorption of Cu (II) and As(V), Chem. Eng. J. 200–202 (2012) 654–662, https://doi.org/10.1016/j.cej.2012.06.126.
[42] C.M. Futalan, C.C. Kan, M.L. Dalida, K.J. Hsien, C. Pascua, M.W. Wan, Comparative and competitive adsorption of copper, lead, and nickel using chitosan immobilized on bentonite, Carbohydr. Polym. 83 (2011) 528–536, https://doi.org/10.1016/j.carbpol.2010.08.013.
[43] F.C.F. Barros, F.W. Sousa, R.M. Cavalcante, T. V Carvalho, F.S. Dias, D.C. Queiroz, L.C.G. Vasconcellos, R.F. Nascimento, Removal of copper, nickel and zinc ions from aqueous solution by chitosan8-hydroxyquinoline beads, Clean-Soil Air Water. 36 (2008) 292–298, doi:10.1002/Clen.200700004.
[44] H. Liu, F. Yang, Y. Zheng, J. Kang, J. Qu, J.P. Chen, Improvement of metal adsorption onto chitosan/Sargassum sp. composite sorbent by an innovative ion-imprint technology, Water Res. 45 (2011) 145–154, https://doi.org/10.1016/j.watres.2010.08.017.
[45] L.-T. Zhang, J. Guo, M. Li, O.B. Tshinkobo, C. Wang, C.-G. Xue, Y. Liu, J.-J. Li, Low-Cost magnetic adsorbent for efficient Cu (II) removal from water, Mater. Res. Express 7 (10) (2020) 105503.
[46] K. Szewczuk-Karpisz, M. Wiśniewska, M. Medykowska, M.V. Galaburda, V. M. Bogatyrov, O.I. Oranska, M. Błachnio, P. Oleszczuk, Simultaneous adsorption of Cu (II) ions and poly(acrylic acid) on the hybrid carbon-mineral nanocomposites with metallic elements, J. Hazard. Mater. 412 (2021) 125138.
[47] K. Parida, K.G. Mishra, S.K. Dash, Adsorption of Copper (II) on NH 2 -MCM-41 and Its Application for Epoxidation of Styrene, Ind. Eng. Chem. Res. 51 (5) (2012) 2235–2246.
[48] A.S. Enshirah Da'na, Adsorption of copper on amine-functionalized SBA-15 prepared by co-condensation : Equilibrium properties, Chem. Eng. J. 166 (2011) 445–453, doi:10.1016/j.cej.2010.11.016.
[49] N. Danesh, M. Ghorbani, A. Marjani, Separation of copper ions by nanocomposites using adsorption process, Sci. Rep. 11 (2021) 1–23, https://doi.org/10.1038/s41598-020-80914-w.
[50] A. Guijarro-Aldaco, V. Hernández-Montoya, A. Bonilla-Petriciolet, M.A. Montes-Morán, D.I. Mendoza-Castillo, Improving the Adsorption of Heavy Metals from Water Using Commercial Carbons Modified with Egg Shell Wastes, Ind. Eng. Chem. Res. 50 (15) (2011) 9354–9362.
[51] X. Chen, G. Chen, L. Chen, Y. Chen, J. Lehmann, M.B. McBride, A.G. Hay, Adsorption of copper and zinc by biochars produced from pyrolysis of hardwood and corn straw in aqueous solution, Bioresour. Technol. 102 (19) (2011) 8877–8884.